

Photon blockade with a four-level quantum emitter coupled to a photonic-crystal nanocavity

M. Bajcsy, A. Majumdar, A. Rundquist and J. Vučković

Ginzton Laboratory, Stanford University, Stanford, CA 94305

E-mail: bajcsy@stanford.edu

Abstract. We study the photon blockade phenomenon in a nanocavity containing a single four-level quantum emitter. By numerically simulating the second-order autocorrelation function of the intra-cavity field with realistic parameters achievable in a state-of-the-art photonic-crystal nanocavity, we show that in the strongly coupled regime the resulting photon blockade is significantly better than that achievable with a two-level emitter. We introduce an intuitive picture of the photon blockade with a four-level emitter that explains the performance difference between the two-level and the four-level emitter schemes, as well as why – in contrast to a cavity containing a two-level atom – signatures of photon blockade appear and should be experimentally observable even outside the strong coupling regime when a four-level emitter is used. Finally, we show that the emitter-cavity coupling achievable in a nanocavity can overcome the non-ideal spacing of optical transitions in realistic four-level emitters that has so far prevented experimental realization of this photon blockade scheme.

PACS numbers: 42.50.Pq, 37.30+i

1. Introduction

In recent years, photon blockade [1] has generated a lot of scientific interest as a promising tool for controllably implementing repulsion-equivalent interactions between photons, which can be used for quantum simulations [2, 3, 4]. Additionally, photon blockade provides a mechanism to coherently generate non-classical light states [5, 6] for applications such as quantum information processing and quantum cryptography [7]. Numerous platforms have been proposed for experimental implementation of photon blockade, such as single quantum emitters in cavity quantum electrodynamics (cQED) systems [8, 1, 9, 10, 11, 12], atoms in Rydberg states [13, 14], and atomic ensembles in photonic waveguides [15]. Experimental demonstrations of photon blockade have so far been achieved for the most part with cQED platforms in the regime of strong coupling. These reports include atomic cQED systems based on a Fabry-Perot cavity [9] and solid-state cQED systems based on single quantum dots embedded in a photonic crystal nanocavity [5, 16]. Additionally, cQED systems achieving photon blockade in the weak coupling regime have been demonstrated with laser cooled atoms coupled to a toroidal microcavity [10] and predicted for quantum dots coupled to either a bimodal nano-cavity [11] or to a photonic molecule [12, 17]. Unfortunately, platforms implementing photon blockade have so far proved to be difficult to scale into more complex systems. Photonic crystal cavities containing strongly-coupled self-assembled quantum dots have shown a lot of promise in this area [18], but further scalability of this platform still remains challenging due to the non-deterministic spatial location and spectral properties of the self-assembled quantum dots. On the other hand, cold atoms are by nature identical, which makes them excellent candidates for quantum emitters in scalable architectures. However, building scalable architecture based on atomic cavity QED systems demonstrated so far is non-trivial. Coupling laser-cooled atoms to planar photonic-crystal cavities was first suggested in Ref. [19] and has been since explored in additional proposals, such as [20, 2]. While experimental realization of these proposals is challenging, recent developments in design of planar photonic-crystal cavities, such as those described in [21, 22, 23] have opened additional prospects of cold atoms interacting with the field maximum of a cavity with a mode volume that is ordinarily associated exclusively with solid-state cQED.

In the experimental demonstrations reported so far, photon blockade was achieved with a two-level quantum emitter (a neutral atom or a quantum dot) coupled to the cavity. However, Imamoglu *et al.* originally coined the term “photon blockade” in a proposal envisioning a four-level atom coupled to a Fabry-Perot cavity [1]. In the strong coupling regime, this scheme was predicted to result in a more robust photon blockade compared to the conventional approach of a two-level emitter coupled to a single mode of a cavity, with quantum interference suggested as a possible cause [24]. In the years following the initial proposal, photon blockade based on a four-level quantum emitter coupled to a cavity has been analyzed extensively [25, 26, 24, 27, 28, 29]. However, these theoretical studies examined the blockade under conditions observed in atomic cQED

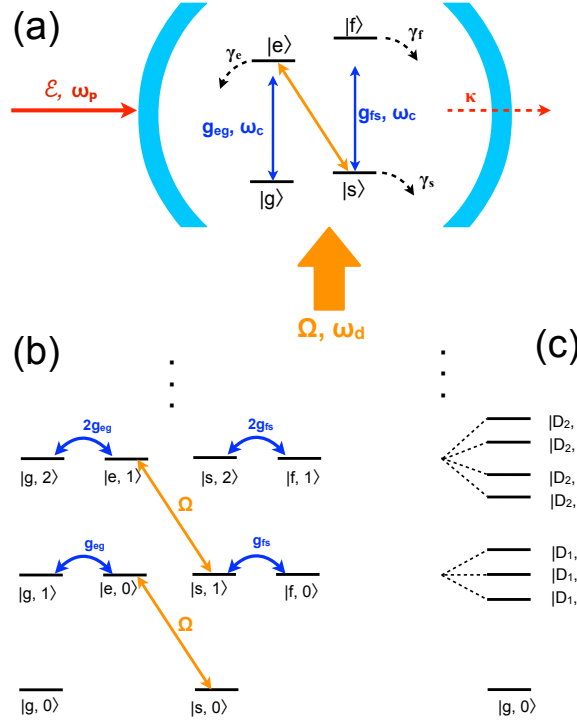


Figure 1. (Color online) (a) Schematics of the described photon blockade system consisting of a four level quantum emitter coupled to a cavity. The cavity is driven by a weak classical probe with frequency ω_p and driving rate \mathcal{E} , while the transitions from $|g\rangle$ to $|e\rangle$ and from $|s\rangle$ to $|f\rangle$ are coupled to the cavity field. Levels $|s\rangle$ and $|e\rangle$ are coupled by a classical field (drive) that does not couple into the cavity and has a frequency ω_d and driving rate Ω . (b) The bare states of the overall system with quantized cavity field and the coupling rates between them. (c) The ground state, first, and second manifold of the dressed states of the overall system for the idealized atom with $\Delta_c = \Delta_{sg} = \Delta_{eg} = \Delta_{fg} = 0$ (i.e., probe resonant with the cavity, drive resonant with the $|e\rangle \rightarrow |s\rangle$ transition, and cavity resonant with $|g\rangle \rightarrow |e\rangle$ and $|s\rangle \rightarrow |f\rangle$ transitions).

experiments in the regime of strong coupling where the rate of atom-field coupling g far exceeds the cavity field decay rate κ and, in most cases, only for idealized atoms with the transitions $|g\rangle \rightarrow |e\rangle$ and $|s\rangle \rightarrow |f\rangle$ (Fig. 1(a)) having the same or nearly the same frequency.

Here, we take a closer look at a four-level quantum emitter coupled to a cavity as shown in Fig. 1(a), in the regime of $g \approx \kappa$ with the cavity mode volume $V_{mod} \sim \lambda^3$, where λ is the wavelength of the probe light. This regime is encountered for self-assembled quantum dots embedded in photonic-crystal microcavities, e.g. [30, 5], and can also be expected for the first generation of experiments coupling laser-cooled atoms to these cavities. Note that as an alternative to being trapped at and interacting with the field maximum of an air-mode cavity, such as those described in [21, 22, 23], the atom could also interact with the evanescent field of a dielectric-mode photonic-crystal cavity while being trapped near the surface of such cavity, e.g. using techniques described in [15] or

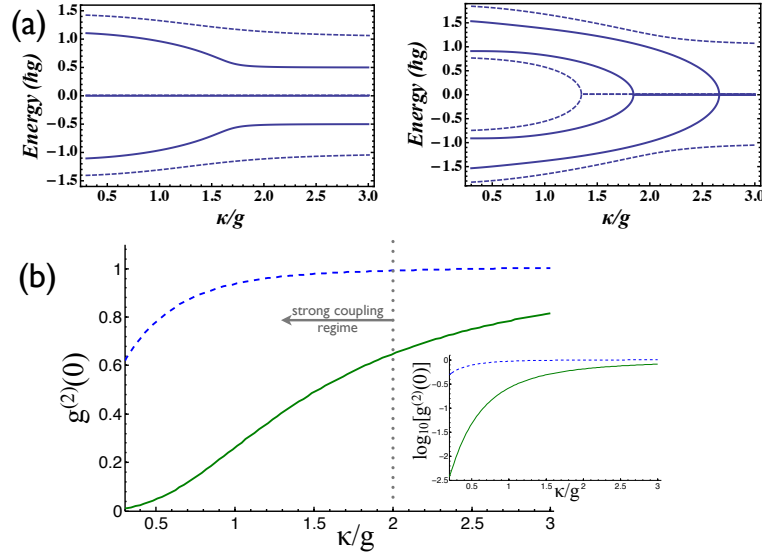


Figure 2. (Color online) (a) Energy splitting of the levels in the first (left) and second (right) manifold of the dressed states for an idealized, i.e. resonant, system with $g_{eg} = g_{fs} = g$. Here, $\Omega = g_{eg}/2$ (solid lines) and $\Omega = g_{eg}$ (dashed lines). $\gamma_e/g = \gamma_f/g = 3 \times 10^{-3}$, $\gamma_s/g = 3 \times 10^{-4}$. (b) Numerical simulation of the second order correlation function $g^{(2)}(0)$ of the light transmitted through such ideal system for $g_{eg}/2\pi = 3$ GHz and $\Omega = g_{eg}$ (green curve) compared to that of a two-level system with the same parameters (blue curve). The inset plots $g^{(2)}(0)$ on a log scale. For both simulations, $\mathcal{E}/2\pi = 0.1$ GHz and the decay rates of the excited states are $2\pi \times 10$ MHz.

in [31, 32].

As a model system for our numerical simulation, we assume a single quantum emitter based on a laser-cooled cesium atom interacting with the field of a solid state nanocavity. However, we emphasize that such four-level systems could in principle also be implemented in solid state. As the system is driven by two classical fields, we monitor the second-order autocorrelation function of the field inside the cavity to study the strength of the photon blockade achievable in a cavity with mode volume comparable to cubed wavelength of the probe light.

2. Basic model

The Hamiltonian describing the coherent dynamics of a system depicted in Fig.1(a) consisting of a four-level emitter and a cavity is given by [24, 25]

$$H = H_o + H_{int} + H_{drive}, \quad (1)$$

where, assuming the rotating wave approximation,

$$\begin{aligned} H_o &= \omega_c a^\dagger a + \omega_{sg} |s\rangle\langle s| + \omega_{eg} |e\rangle\langle e| + \omega_{fg} |f\rangle\langle f| \\ H_{int} &= g_{eg} (a^\dagger |g\rangle\langle e| + a |e\rangle\langle g|) + g_{fs} (a^\dagger |s\rangle\langle f| + a |f\rangle\langle s|) \end{aligned}$$

$$\begin{aligned}
& + \Omega e^{-i\omega_d t} |e\rangle\langle s| + \Omega^* e^{i\omega_d t} |s\rangle\langle e| \\
H_{drive} &= \mathcal{E} e^{-i\omega_p t} a^\dagger + \mathcal{E}^* e^{i\omega_p t} a.
\end{aligned}$$

In this description, a is the annihilation operator for the cavity mode, and the classical weak probe field couples to the cavity at a rate \mathcal{E} . Another classical field with polarization orthogonal to the polarization of the cavity mode provides coupling between levels $|s\rangle$ and $|e\rangle$ with Rabi frequency Ω without directly injecting photons into the cavity mode. The field of the cavity mode couples levels $|g\rangle$ and $|e\rangle$ and levels $|s\rangle$ and $|f\rangle$ with rates g_{eg} and g_{fs} , respectively. In the above equations, ω_c is the frequency of the cavity mode and ω_{ij} are the frequencies of the atomic transition from level $|j\rangle$ to level $|i\rangle$ in Fig. 1(a) and \hbar is set to 1. This analysis is relevant for any single-mode cavity, and does not involve any typical characteristics of a nanocavity. By transforming into a rotating frame, the original Hamiltonian will change into

$$\mathcal{H} = U^\dagger H U + i \frac{dU^\dagger}{dt} U = \mathcal{H}_o + \mathcal{H}_{int} + \mathcal{H}_{drive}, \quad (2)$$

with

$$\begin{aligned}
U &= e^{-i[\omega_p(a^\dagger a + |e\rangle\langle e|) + (\omega_p - \omega_d)|s\rangle\langle s| + (2\omega_p - \omega_d)|f\rangle\langle f|]} \\
\mathcal{H}_o &= -\Delta_c a^\dagger a - \Delta_{sg}|s\rangle\langle s| - \Delta_{eg}|e\rangle\langle e| - \Delta_{fg}|f\rangle\langle f| \\
\mathcal{H}_{int} &= g_{eg}(a^\dagger|g\rangle\langle e| + a|e\rangle\langle g|) + g_{fs}(a^\dagger|s\rangle\langle f| + a|f\rangle\langle s|) \\
&\quad + \Omega|e\rangle\langle s| + \Omega^*|s\rangle\langle e| \\
\mathcal{H}_{drive} &= \mathcal{E} a^\dagger + \mathcal{E}^* a,
\end{aligned}$$

where $\Delta_c = \omega_p - \omega_c$, $\Delta_{sg} = \omega_p - \omega_{sg} - \omega_d$, $\Delta_{eg} = \omega_p - \omega_{eg}$, $\Delta_{fg} = 2\omega_p - \omega_d - \omega_{fg}$. In the limit of a very weak probe field ($\mathcal{E} \rightarrow 0$), the couplings between the bare states of the lowest manifolds of the overall system are depicted in Fig. 1 (b), where each bare state is described by the state of the atom and the number of photons present in the cavity mode. The new eigenstates of the system are sketched in Fig. 1 (c) for the resonant case ($\Delta_c = \Delta_{sg} = \Delta_{eg} = \Delta_{fg} = 0$). The number of these dressed states in each manifold provides an intuitive explanation of the mechanism behind the photon blockade in this system. Specifically, if the probe is resonant with the bare cavity, the first photon will be resonant to the $|g, 0\rangle \rightarrow |D_1, 0\rangle$ transition, while the second photon will be out of resonance with any transition available out of state $|D_1, 0\rangle$ [24, 25]. If we take into account the dissipation of the cavity field to the environment with a decay rate κ and the spontaneous decay rates between the atomic levels γ_{sg} , γ_{eg} , γ_{es} , γ_{fg} , and γ_{fs} , we can describe the dynamics of system with a master equation

$$\frac{d\rho}{dt} = -\frac{i}{\hbar}[\mathcal{H}, \rho] + 2\kappa\mathcal{L}[a] + 2\sum_{ij}\gamma_{ij}\mathcal{L}[\sigma_{ij}], \quad (3)$$

where ρ is the system's density matrix, $ij \in \{sg, eg, es, fg, fs\}$ and $\sigma_{ij} = |j\rangle\langle i|$. $\mathcal{L}[D]$ is the Lindblad superoperator on operator D used to model the incoherent decays and is given by

$$\mathcal{L}[D] = D\rho D^\dagger - \frac{1}{2}D^\dagger D\rho - \frac{1}{2}\rho D^\dagger D. \quad (4)$$

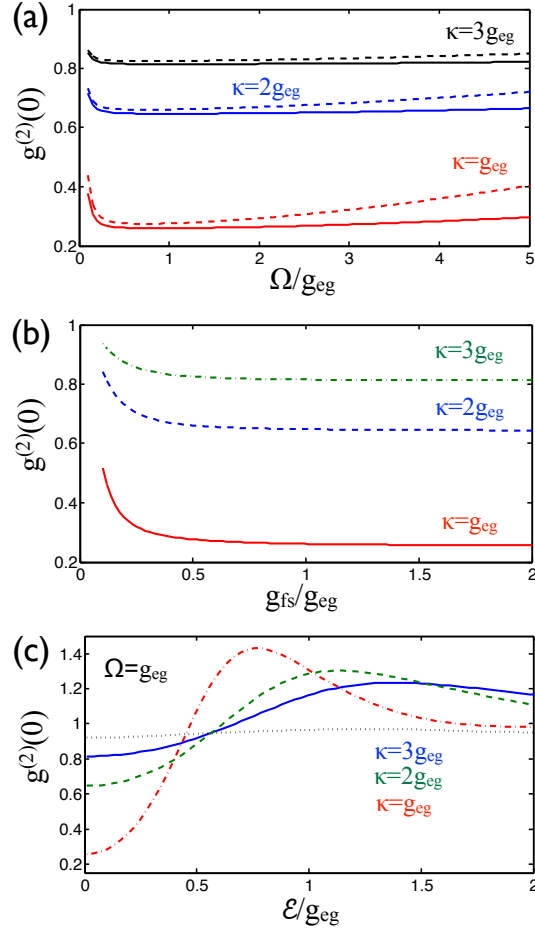


Figure 3. (Color online) (a) A numerical simulation of the second order correlation function $g^{(2)}(0)$ of the light transmitted through the resonant system as a function of the amplitude of the classical field Ω with respect to g_{eg} for different values of κ . Here, $g_{eg}/2\pi = 3$ GHz, $\mathcal{E}/2\pi = 0.1$ GHz, $g_{fs} = g_{eg}$ (solid curves), $g_{fs} = g_{eg}/2$ (dashed curves). (b) Numerically simulated $g^{(2)}(0)$ as a function of g_{fs}/g_{eg} for $g_{eg}/2\pi = 3$ GHz, $\mathcal{E}/2\pi = 0.1$ GHz, and $\Omega = g_{eg}/2$. (c) Numerically simulated $g^{(2)}(0)$ as a function of the amplitude of the probe field \mathcal{E} for $g_{eg}/2\pi = 3$ GHz, $\Omega = g_{eg}$. The value of κ in this simulation is $3g_{eg}$ (solid blue curve), $2g_{eg}$ (dashed green curve), and g_{eg} (dash-dot red curve). For comparison, the dotted black curve plots $g^{(2)}(0)$ as a function of \mathcal{E} for photon blockade with a two level quantum emitter in a cavity with $\kappa = g_{eg}$. In all three parts of the figure, $\gamma_{eg} = \gamma_{es} = \gamma_{fg} = \gamma_{fs} = 2\pi \times 10$ MHz and $\gamma_{sg} = 2\pi \times 1$ MHz.

For simplicity, we will ignore additional decay mechanisms and set $\gamma_s = \gamma_{sg}$, $\gamma_e = \gamma_{eg} + \gamma_{es}$, and $\gamma_f = \gamma_{fg} + \gamma_{fs}$ (Fig. 1 (a)). We numerically simulate the dynamics of the system described by equation (3) using the routines provided in the quantum optics toolbox [33] with up to six-photon Fock states.

3. Fully resonant case

We start by looking at the idealized case of a fully resonant system ($\Delta_c = \Delta_{sg} = \Delta_{eg} = \Delta_{fg} = 0$). This fully resonant case has been explored in detail in previous works [24, 25, 27, 28, 29] with parameters corresponding to atomic cQED experiments in Fabry-Perot cavities ($g_{eg}/2\pi = 120$ MHz) [34] in the regime of strong coupling ($g_{eg} > 5\kappa$). Here, we revisit the resonant case but perform our numerical simulations with parameters that can be expected for a system based on a photonic crystal microcavity, in particular $g_{eg}/2\pi = 3$ GHz. This is a fairly conservative value for atom-photon coupling achievable in a photonic-crystal nano-cavity, as values of $2\pi \times 17$ GHz have been predicted by Lev *et al.* [20] for closed transitions in cesium. We choose the lower value to budget for experimental imperfections, such as the possible use of cavity designs with larger mode volume, the use of weaker transitions to implement the four level emitter in a realistic atom, and the atom not being localized in the cavity field maximum, perhaps due to the atom's thermal motion or because the atom is trapped above the surface of the photonic crystal. For the cavity field decay, we focus on the interval of $\kappa/2\pi \approx 1 - 10$ GHz, corresponding to quality factors of $Q \sim 3 \times 10^4$ to 3×10^5 . For the chosen value of g_{eg} , this range includes the transition point $g_{eg} \approx \frac{\kappa}{2}$ between the weak and strong atom-field coupling in the cavity. Values from this range have been observed in solid state cQED experiments in GaAs cavities [5, 30], and values of Q even higher have been predicted for air-mode cavities fabricated in other materials [22]. Particular materials of interest would include GaP [35], SiN, GaN, and SiO₂ [36], as these – unlike GaAs – remain transparent for light at wavelengths corresponding to commonly used optical transitions of alkali metals.

The energy splittings of the dressed states in the first and second manifold are plotted as a function of the cavity field decay κ in Fig. 2 (a). These plots were obtained by numerically evaluating and then plotting the real part of the eigenvalues of the Hamiltonian \mathcal{H} from equation (2) with complex detunings to include the decay mechanisms [27]. For the chosen parameters, the first manifold is symmetrically split into three levels, with one of the levels remaining at the energy of the original bare cavity. Qualitatively, the behavior of the first manifold is relatively insensitive to the value of κ and Ω . On the other hand, the second manifold splits into three and eventually into four distinct energy levels with a decreasing value of κ , while the value of κ at which these splits occur can be affected by changing the ratio between g_{eg} and Ω .

The effects of this level structure on the photon statistics inside the cavity can be seen in Fig. 2 (b), where we plot the second order correlation function $g^{(2)}(0)$ of the field inside the cavity as a function of the g/κ ratio with the probe field resonant with the bare cavity ($\Delta_c = 0$, green curve). We see that, in a fashion similar to schemes based on a two-level emitter coupled to a bimodal cavity [10, 11], the photons become anti-bunched ($g^{(2)}(0) < 1$) already for $g_{eg} < \frac{\kappa}{2}$, i. e. before strongly coupled regime is reached. This is particularly interesting when compared to the energy splittings of the dressed states plotted in Fig. 2 (a), since one would not expect a blockade until the energy degeneracy

of the bare states is lifted by strong enough emitter-field coupling. For comparison, we also plot the $g^{(2)}(0)$ expected for a two-level atom coupled to a cavity with identical parameters and probe detuning optimized for this system (blue curve, $\Delta_c \approx 1.5g$). The anti-bunching resulting from a four-level system is much stronger than that achievable in a two-level system, with the difference exceeding two orders of magnitude for $g/\kappa > 5$ (Fig. 2(b), inset). This is similar to predictions made based on parameters achievable in a Fabry-Perrot cavity [24].

In Fig. 3, we numerically simulate the effects of the system's key parameters on the photon statistics. For a given value of κ , the resulting $g^{(2)}(0)$ is fairly robust against variations in the magnitude of the coherent field Ω (Fig. 3 (a)). Similarly, $g^{(2)}(0)$ remains nearly constant for $g_{fs} > g_{eg}/2$ (Fig. 3 (b)). Lastly, the light inside the cavity remains anti-bunched for a broad range of values of the probe field amplitude (Fig. 3 (c)), before changing into the bunching regime predicted in [29].

4. The intuitive picture

An intuitive picture of why a significantly better photon blockade is expected with a four-level emitter can be provided by comparing the transmission of the system for the first photon and for the second photon coupled into the cavity. An estimate of these transmissions can be obtained by taking the non-Hermitian Hamiltonians characterizing

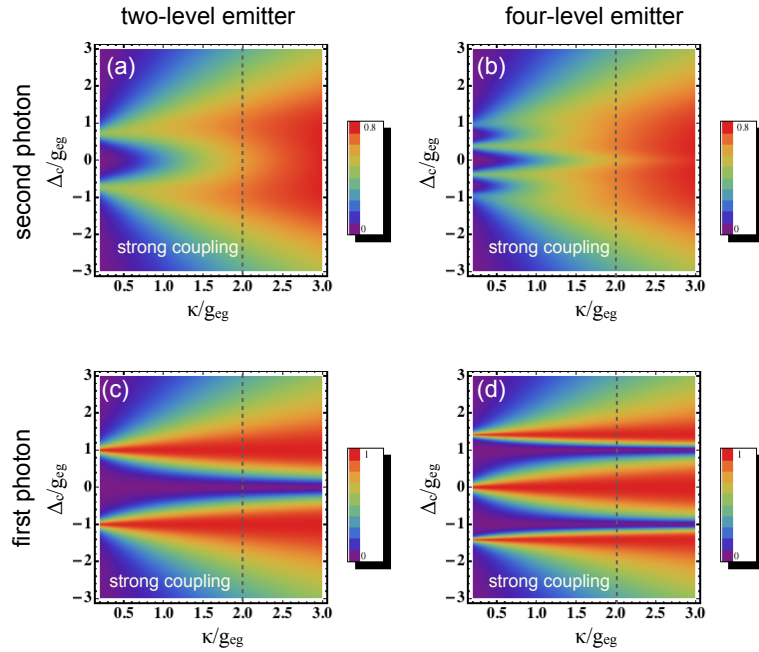


Figure 4. Estimated transmission of the first two photons through a cavity with a resonant quantum emitter as a function of probe detuning: (a) and (c) for the case of a two-level emitter ($\Delta_{eg} = \Delta_c$); (b) and (d) for an ideal four-level emitter ($\Delta_{eg} = \Delta_{fs} = \Delta_c$) with parameters from Fig 2 (b). The border of the strong coupling regime for the $|g\rangle \rightarrow |e\rangle$ transition is marked by the vertical dashed line in each plot.

the system's transition between its ground and first, as well as first and second manifolds, applying these Hamiltonians to wave-functions describing the system state in these manifolds, and then finding a steady-state solution under the condition of a weak probe field.

The non-Hermitian Hamiltonian describing the system's transition between the ground state and the first manifold can be written as

$$\begin{aligned}\tilde{\mathcal{H}}^{(1)} = & - (i\kappa + \Delta_c)a^\dagger a - (i\gamma_{sg} + \Delta_{sg})|s\rangle\langle s| \\ & - (i\gamma_{eg} + \Delta_{eg})|e\rangle\langle e| + g_{eg}(a^\dagger|g\rangle\langle e| + a|e\rangle\langle g|) \\ & + \Omega|e\rangle\langle s| + \Omega^*|s\rangle\langle e| + \mathcal{E}a^\dagger + \mathcal{E}^*a.\end{aligned}\quad (5)$$

If we assume the system is in a state described by

$$|\psi^{(1)}\rangle = c_o^{(1)}|g, 0\rangle + c_1^{(1)}|g, 1\rangle + c_2^{(1)}|e, 0\rangle + c_3^{(1)}|s, 0\rangle, \quad (6)$$

then the equation we are trying to solve is

$$i\frac{d}{dt}|\psi^{(1)}\rangle = \tilde{\mathcal{H}}^{(1)}|\psi^{(1)}\rangle. \quad (7)$$

In the limit of $\mathcal{E} \rightarrow 0$, we set $c_o^{(1)} \approx 1$ and we neglect the manifold-connecting effects of the probe, such as the $|g, 1\rangle \rightarrow |g, 2\rangle$, $|e, 0\rangle \rightarrow |e, 1\rangle$, $|s, 0\rangle \rightarrow |s, 1\rangle$ coupling. We define the transmission of the first photon through the system as

$$T^{(1)} = \frac{\langle a^\dagger a \rangle}{\langle a^\dagger a \rangle_o^{(1)}} \approx \frac{|c_1^{(1)}|^2}{|\mathcal{E}|^2} \kappa^2, \quad (8)$$

with $\langle a^\dagger a \rangle_o^{(1)}$ being the transmission of the first photon through an empty cavity on resonance, and solve equation (7) in steady state ($\frac{d}{dt}c_j^{(1)} = 0$) to find the value of $c_1^{(1)}$.

In a similar fashion, the non-Hermitian Hamiltonian describing the system's transition between the first and second manifold can be written as

$$\tilde{\mathcal{H}}^{(2)} = \tilde{\mathcal{H}}^{(1)} - (i\gamma_{fs} + \Delta_{fs})|f\rangle\langle f| + g_{fs}(a^\dagger|s\rangle\langle f| + a|f\rangle\langle s|). \quad (9)$$

We assume the system is in a state described by

$$|\psi^{(2)}\rangle = c_o^{(2)}|g, 1\rangle + c_1^{(2)}|g, 2\rangle + c_2^{(2)}|e, 1\rangle + c_3^{(2)}|s, 1\rangle + c_4^{(2)}|f, 0\rangle \quad (10)$$

and we are trying to extract the information about the transmission encountered by the second photon (assuming the first photon has already coupled into the system) by solving the equation

$$i\frac{d}{dt}|\psi^{(2)}\rangle = \tilde{\mathcal{H}}^{(2)}|\psi^{(2)}\rangle. \quad (11)$$

Again, in the limit of $\mathcal{E} \rightarrow 0$, we set $c_o^{(2)} \approx 1$, neglect the manifold-connecting effects of the probe, define the transmission of the second photon as

$$T^{(2)} = \frac{\langle a^\dagger a \rangle}{\langle a^\dagger a \rangle_o^{(2)}} \approx 2\frac{|c_1^{(2)}|^2}{|\mathcal{E}|^2} \kappa^2, \quad (12)$$

with $\langle a^\dagger a \rangle_o^{(2)}$ being the transmission of the first photon through an empty cavity on resonance, and solve equation (11) in steady state to find the value of $c_1^{(2)}$.

An analogous approach can be used to estimate the transmission of the first and second photon through a cavity with a two-level emitter. The result of that calculation is plotted in Fig. 4 (a) and (c) for comparison with the four-level emitter case. We see that deep in the strongly coupled regime ($\kappa = g_{eg}/3$ in Fig. 5 (c)) the best transmission of the first photon is achieved for $|\frac{\Delta_c}{g_{eg}}| = 1$, while the transmission of the second photon at this detuning is significantly suppressed (Fig. 4 (a)). Unfortunately, with increasing cavity field decay κ , the transmission of the second photon increases for $|\Delta_c| = g_{eg}$. One can remain in the photon blockade regime by adjusting the frequency of the probe – effectively trading off the transmission of the first photon for reduced transmission of the second photon – until the transmission peaks of the second photon become too broad and adjusting Δ_c will not have a noteworthy effect on the statistics of the transmitted light anymore.

Returning to the ideal four-level emitter, we see that when the probe is resonant with the bare cavity ($\Delta_c = 0$, Fig. 4 (d)) the transmission of the first photon is maximized, while at the same time there is a minimum in the transmission of the second photon (Fig. 4 (b)). This convenient frequency alignment of the maximum transmission for the first photon with a local minimum in the transmission of the second photon is present even outside the strongly coupled regime and while the energies of the dressed states (Fig. 2(a)) remain degenerate. This minimum can be thought of as a generalized case of dipole induced transparency (DIT) [37] and a similar minimum in the transmission of the second photon at $\Delta_c = 0$ can be observed in the case of a two-level emitter (Fig. 4 (a)). In this case though, this minimum coincides with a minimum in the transmission of the first photon (Fig. 4 (c)) and is therefore not useful for implementing photon blockade.

To summarize, the optimal frequency alignment of the maximum transmission for the first photon with a local minimum in the transmission of the second photon provides an intuitive explanation for the superior photon blockade performance of the four-level emitter.

5. Off-resonant system

While the fully-resonant system is interesting as a model for understanding the mechanisms behind the photon blockade and for estimating the limits of its behavior, a practical implementation of this scheme will most likely have to be done with a four-level quantum emitter in which the frequencies of the $|g\rangle \rightarrow |e\rangle$ and $|s\rangle \rightarrow |f\rangle$ transitions differ significantly. For example, in the alkali atoms used commonly for cQED experiments, such as rubidium or cesium, the frequency difference between these two transitions is about two orders of magnitude larger than the atom-field coupling rate g achieved in current experimental atomic cQED systems [9, 10, 38], which report $g/2\pi \sim 10 - 100$ MHz. The only exceptions are disk cavities reported by Barclay *et al.* [39], who predict $g/2\pi \approx 0.9$ GHz for atoms displaced 100 nm from the cavity surface. However, coupling of atoms to these cavities has not yet been demonstrated to the best

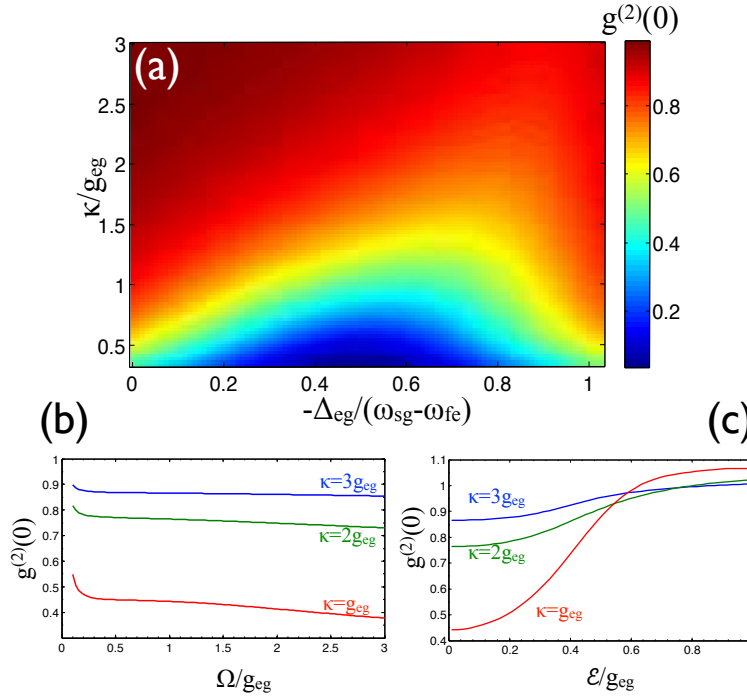


Figure 5. (Color online) (a) Numerical simulation of $g^{(2)}(0)$ as a function of cavity decay rate κ and probe detuning Δ_{eg} from the $|g\rangle \rightarrow |e\rangle$ transition in a four-level system based on ^{133}Cs ($\omega_{sg} - \omega_{fe} = 2\pi \times 8.941$ GHz). Here, the probe is resonant with the cavity ($\Delta_c = 0$) and we keep $\Delta_{sg} = 0$ by setting $\omega_d = \omega_p - \omega_{sg}$. $g_{eg}/2\pi = 3$ GHz, $g_{fs} = 1.5g_{eg}$, $\Omega = g_{eg}$. (b) $g^{(2)}(0)$ as a function of the amplitude of the classical field Ω for different values of κ . (c) Effects of the probe field amplitude \mathcal{E} on $g^{(2)}(0)$. In both (b) and (c) the value of Δ_{eg} is chosen to minimize $g^{(2)}(0)$. In all plots, $\gamma_{eg} = \gamma_{es} = \gamma_{fg} = \gamma_{fs} = 2\pi \times 10$ MHz and $\gamma_{sg} = 2\pi \times 1$ MHz.

of our knowledge.

In this section, we therefore base the four-level quantum emitter on the ^{133}Cs atom, in which $\omega_{sg} - \omega_{fe} \approx 2\pi \times 8.941$ GHz, to study the photon blockade under conditions that are closer a realistic system. Of course this representation of the cesium atom, while maintaining the frequency scales, is still highly simplified. To study this system in detail one needs to implement a full simulation including the effects of all participating levels of the cesium atom in a fashion similar to the work presented by Birnbaum *et al.* [40].

Following the approach suggested by Greentree *et al.* [27], we keep the probe resonant with the cavity, adjust ω_d to stay on resonance with the two-photon transition $|g\rangle \rightarrow |s\rangle$ ($\omega_d = \omega_p - \omega_{sg}$), and vary the probe detuning Δ_{eg} from the $|g\rangle \rightarrow |e\rangle$ transition. In this approach, the probe can couple well into the cavity, while adjusting Δ_{eg} optimizes the strength of the interaction of the cavity photons with the two cavity-coupled transitions $|g\rangle \rightarrow |e\rangle$ and $|s\rangle \rightarrow |f\rangle$. Figure 5(a) then plots $g^{(2)}(0)$ as a function of cavity decay rate κ and probe detuning Δ_{eg} from the $|g\rangle \rightarrow |e\rangle$ transition for a probe resonant with the cavity ($\Delta_c = 0$). We see that for each value of κ within the

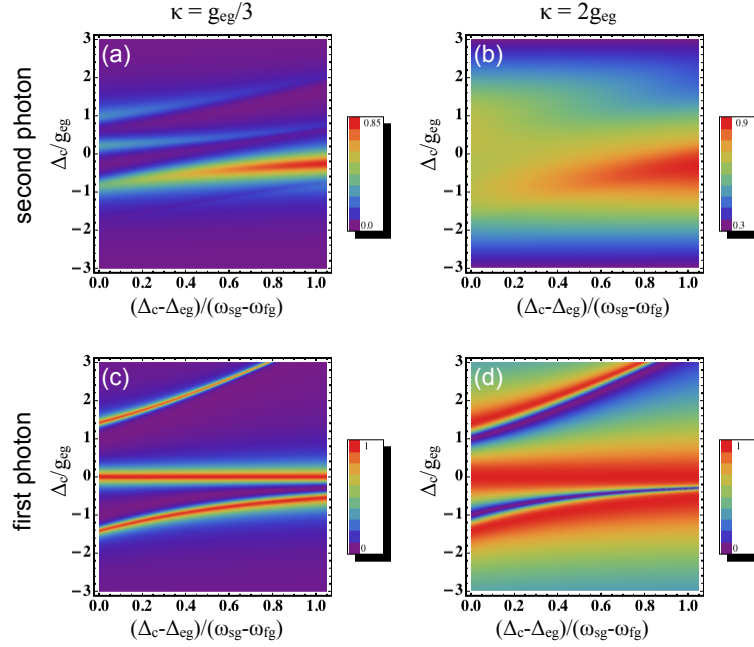


Figure 6. Estimated transmission of the first two photons through the system numerically simulated in Fig. 5 as a function of detuning Δ_c of the probe from the cavity: (a) and (c) for the case of strong coupling regime between the emitter and the cavity ($\kappa = g_{eg}/3$); (b) and (d) for the system being on the verge of strong coupling regime ($\kappa = 2g_{eg}$).

range under consideration, there is an interval of Δ_{eg} for which the light inside the cavity becomes anti-bunched ($g^{(2)}(0) < 1$). Similarly, as in the case of the ideal atom, changing the value of Ω affects blockade only slightly (Fig. 5(b)) and the light inside the cavity remains anti-bunched for a relatively wide range of intensities of the probe light (Fig. 5(c)). Note that both of these plots display the minimum value of $g^{(2)}(0)$ for a given Ω or \mathcal{E} that can be achieved by adjusting Δ_{eg} while keeping the probe resonant with the cavity.

The effects of adjusting Δ_{eg} on the photon blockade in an off-resonant system can also be observed in the intuitive picture described in the previous section. Figure 6 plots the estimated transmission for the first and second photon through the system numerically simulated in Fig. 5 (a) for strong coupling regime ($\kappa = g_{eg}/3$) and outside of strong coupling regime ($\kappa = 2g_{eg}$). In both cases we see that the transmission of the first photon remains highest at $\Delta_c = 0$ as the detuning of the probe Δ_{eg} from the $|g\rangle \rightarrow |e\rangle$ transition is changed (Fig. 6 (c), (d)). On the other hand, there is a minimum with respect to Δ_{eg} in the transmission of the second photon when $\Delta_c = 0$. This minimum is particularly pronounced in the strong coupling regime (Fig. 6 (a)) and remains present, although in a washed-out form, even as the cavity decay is increased to $\kappa = 2g_{eg}$ (Fig. 6 (b)). However, terms of the value of Δ_{eg} at which the minimum happens, the agreement with the numerical simulation in Fig. 5 is only qualitative, most likely due to the manifold-connecting effects of the probe field \mathcal{E} that are neglected in

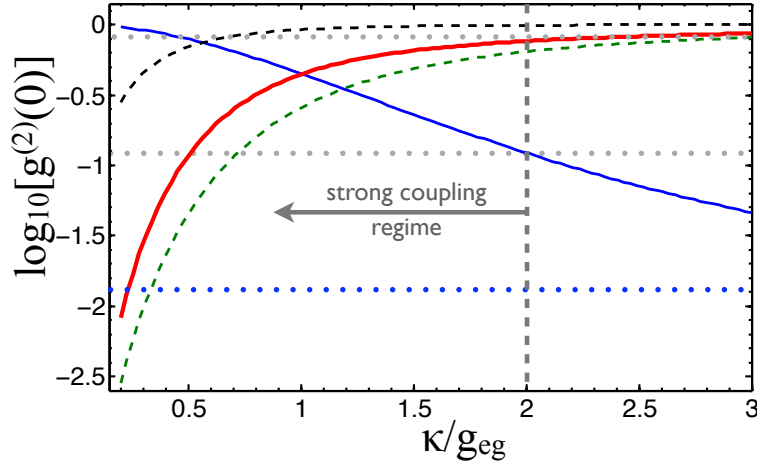


Figure 7. (Color online) Comparison of $g^{(2)}(0)$ achievable with a four-level off-resonant emitter based on cesium (solid red curve) with a resonant four-level emitter from Fig. 2(c) (dashed green), with a comparable two-level emitter (dashed black curve), and with a two-level atom coupled to a bimodal cavity (solid blue curve and dotted blue horizontal line). The two dotted horizontal grey lines correspond to blockade with a four-level off-resonant emitter based on cesium and parameters demonstrated in current cQED experiments: $g_{eg}/2\pi = 120$ MHz, $\kappa/2\pi = 40$ MHz and 4 MHz for the upper and lower grey line, respectively. The decay rates of the atomic excited states are equal for all plots.

the intuitive picture.

The photon blockade achievable with the cesium-based four-level atom is put into perspective in Fig. 7. The solid red curve plots the minimum value of $g^{(2)}(0)$ from Fig. 5(a) as a function of κ . We see that the blockade is slightly worse than that achievable with the ideal resonant system (green dashed curve), but it still vastly outperforms the blockade achievable in an identical cavity with a comparable two level atom (black dashed curve). For comparison, the two grey dotted lines mark the expected blockade with a four-level cesium-based atom and cavities with mode volume resulting in $g_{eg}/2\pi \approx 100$ MHz, which roughly represent state of the art cavities used in atomic cQED experiments, such as [34, 41, 42]. The upper line corresponds to $\kappa/2\pi = 40$ MHz achieved by Hood *et al.* [34], while the lower line represents $\kappa/2\pi = 4$ MHz, which is about five-times smaller than the field decay rate reported by Alton *et al.* [42]. Finally, the solid blue line represents the $g^{(2)}(0)$ expected with a two-level emitter coupled to two orthogonally polarized modes of a degenerate bimodal nanocavity as proposed by Majumdar *et al.* [11], with the blue dashed line marking the lower limit of $g^{(2)}(0)$ in such system. We see that this proposal provides photon-blockade performance comparable to the four-level atom scheme analyzed here, but its implementation with atoms might be difficult due to the selection rules of atomic transitions.

6. Outlook

In conclusion, our results show that, under conditions achievable with currently available photonic crystal nanocavities, the originally proposed photon blockade [1] should be experimentally observable with realistic four-level atoms and even without achieving the strong coupling regime between the atom and the cavity field. The potential for scalability of this scheme when implemented with cold atoms and photonic crystal nanocavities, as well as the robustness to variations in experimental parameters seen in the presented simulations, make the “original” photon blockade a great candidate for experimental realization of networks of coupled nonlinear cavities in which the interactions between photons can be engineered [2].

Additionally, the results presented here might be relevant for exploration of photon blockade with four-level solid state emitters coupled to nanocavities, such as nitrogen-vacancy centers in diamond [43, 44, 45] and charged quantum dots in a strong magnetic field [46].

7. Acknowledgements

This work was supported by DARPA, grant number N66001-12-1-4011. A. R. was also supported by a Stanford Graduate Fellowship.

References

- [1] Imamoglu A, Schmidt H, Woods G and Deutsch M 1997 *Physical Review Letters* **79** 1467–1470
- [2] Greentree A D, Tahan C, Cole J H and Hollenberg L C L 2006 *Nature Phys.* **2** 856
- [3] Hartmann M J, Brandão F G S and Plenio M B 2006 *Nature Phys.* **2** 849
- [4] Carusotto I and Ciuti C 2012 *arXiv* 1205.6500
- [5] Faraon A, Fushman I, Englund D, Stoltz N, Petroff P and Vučković J 2008 *Nat. Phys.* **4** 859–863
- [6] Majumdar A, Bajcsy M and Vučković J 2012 *Phys. Rev. A* **85**
- [7] O’Brien J L, Furusawa A and Vučković J 2009 *Nat. Photonics* **3** 687–695
- [8] Tian L and Carmichael H J 1992 *Phys. Rev. A* **46** 6801–6804
- [9] Birnbaum K M, Boca A, Miller R, Boozer A D, Northup T E and Kimble H J 2005 *Nature* **436** 87
- [10] Dayan B, Parkins A S, Aok T, Ostby E, Vahala K and Kimble H 2008 *Science* **319** 1062–1065
- [11] Majumdar A, Bajcsy M, Rundquist A and Vučković J 2012 *Phys. Rev. Lett.* **108** 183601
- [12] Liew T C H and Savona V 2010 *Phys. Rev. Lett.* **104**
- [13] Gorshkov A V, Otterbach J, Fleischhauer M, Pohl T and Lukin M D 2011 *Phys. Rev. Lett.* **107** 133602
- [14] Peyronel T, Firstenberg O, Liang Q, Hofferberth S, Gorshkov A V, Pohl T, Lukin M D and Vuletić V 2012 *Nature* **488** 57
- [15] Chang D, Gritsev V, Morigi G, Vuletić V, Lukin M and Demler E 2008 *Nature Physics* **4** 884 – 889
- [16] Reinhard A, Volz T, Badolato A, Hennessy K J, Hu E L and Imamoglu A 2012 *Nat. Photonics* **6** 93
- [17] Bamba M, Imamoglu A, Carusotto I and Ciuti C 2011 *Phys. Rev. A* **83** 021802(R)
- [18] Faraon A, Majumdar A, Englund D, Kim E, Bajcsy M and Vučković J 2011 *New Journal of Physics* **13** 055025

- [19] Vučković J, Lončar M, Mabuchi H and Scherer A 2001 *Phys. Rev. E* **65** 016608
- [20] Lev B, Srinivasan K, Barclay P, Painter O and Mabuchi H 2004 *Nanotechnology* **15** S556
- [21] Yamamoto T, Notomi M, Taniyama H, Kuramochi E, Yoshikawa Y, Torii Y and Kuga T 2008 *Optics Express* **16** 13809–13817
- [22] Quan Q and Loncar M 2011 *Optics Express* **19** 18529
- [23] Li J, Fattal D, Fiorentino M and Beausoleil R G 2011 *Phys. Rev. Lett.* **106** 193901
- [24] Werner M J and Imamoglu A 1999 *Phys. Rev. A* **61** 011801(R)
- [25] Rebić S, Tan S M, Parkins A and Walls D F 1999 *J. Opt. B: Quantum Semiclass. Opt* **490**
- [26] Gheri K M, Alge W and Grangier P 1999 *Phys. Rev. A* **60** R2673
- [27] Greentree A D, Vaccaro J A, Echaniz R D, Durrant A V and Marangos J P 2000 *J. Opt. B: Quantum Semiclass. Opt.* **2** 252
- [28] Rebić S, Parkins A S and Tan S M 2002 *Phys. Rev. A* **65** 043806
- [29] Rebić S, Parkins A S and Tan S M 2002 *Phys. Rev. A* **65** 063804
- [30] Hennessy K, Badolato A, Winger M, Gerace D, Atatüre M, Gulde S, Fält S, Hu E L and Imamoglu A 2007 *Nature* **445** 896
- [31] Dawkins S T, Mitsch R, Reitz D, Vetsch E and Rauschenbeutel A 2011 *Phys. Rev. Lett.* **107** 243601
- [32] Lacroûte C, Choi K S, Goban A, Alton D J, Ding D, Stern N P and Kimble H J 2012 *New Journal of Physics* **14** 023056
- [33] Tan S M 1999 *J. Opt. B: Quantum Semiclass. Opt* **1** 424
- [34] Hood C J, Chapman M S, Lynn T W and Kimble H J 1998 *Phys. Rev. Lett.* **80** 4157
- [35] Rivoire K, Faraon A and Vučković J 2008 *Appl. Phys. Lett.* **93** 063103
- [36] Gong Y, Ishikawa S, Cheng S L, Gunji M, Nishi Y and Vučković J 2010 *Phys. Rev. B* **81** 235317
- [37] Waks E and Vučković J 2006 *Phys. Rev. Lett.* **96** 153601
- [38] Koch M, Sames C, Balbach M, Chibani H, Kubanek A, Murr K, Wilk T and Rempe G 2011 *Phys. Rev. Lett.* **107** 023601
- [39] Barclay P E, Srinivasan K, Painter O, Lev B and Mabuchi H 2006 *Appl. Phys. Lett.* **89** 131108
- [40] Birnbaum K M, Parkins A S and Kimble H J 2006 *Phys. Rev. A* **74** 063802
- [41] Aoki T, Parkins A S, Alton D J, Regal C A, Dayan B, Ostby E, Vahala K J and Kimble H J 2009 *Phys. Rev. Lett.* **102** 083601
- [42] Alton D J, Stern N P, Aoki T, Lee H, Ostby E, Vahala K J and Kimble H J 2010 *Nat. Phys.* **7** 159
- [43] Faraon A, Barclay P E, Santori C, Fu K M C and Beausoleil R G 2011 *Nat. Photonics* **5** 301
- [44] Babinec T M, Choy J T, Smith K J M, Khan M and Lončar M 2011 *J. Vac. Sci. Technol. B* **29** 010601
- [45] Englund D, Shields B, Rivoire K, Hatami F, Vučković J, Park H and Lukin M 2010 *Nano Letters* **10** 3922
- [46] Press D, Ladd T D, Zhang B and Yamamoto Y 2008 *Nature* **456** 218